Nanoscale

PAPER

View Article Online
View Journal | View Issue

Cite this: *Nanoscale*, 2018, **10**, 13767

2D SnSe-based vdW heterojunctions: tuning the Schottky barrier by reducing Fermi level pinning†

Wenyang Zhou,[a,b] Yaguang Guo,[a,b] Jie Liu,[a,b] Fancy Qian Wang,[a,b] Xiaoyin Li[a,b] and Qian Wang *[a,b]

Two-dimensional (2D) SnSe is a very promising material for semiconducting devices due to its novel properties. However, the contact behavior between a 2D SnSe sheet and a three-dimensional (3D) metal surface shows an un-tunable Schottky barrier because of the metallization of the SnSe sheet induced by strong Fermi level pinning at the contact interface. In this work, we use graphene rather than 3D metals as the metal electrode which comes into contact with a single-layer SnSe sheet to form a van der Waals (vdW) heterojunction. Based on state-of-the-art theoretical calculations, we find that the intrinsic properties of the SnSe sheet are preserved and the Fermi level pinning is weakened because of the vdW interaction between the SnSe sheet and graphene. We further demonstrate that an Ohmic contact can be realized by doping graphene with boron or nitrogen atoms or using other high-work-function 2D metals such as ZT-$MoSe_2$, ZT-MoS_2, or H-NbS_2 sheet as the electrode to reduce the Fermi level pinning, leading to a spontaneous hole injection from the electrode to the channel material. This study sheds light on how to tune the Schottky barrier height for better device performance.

Received 9th April 2018,
Accepted 21st June 2018

DOI: 10.1039/c8nr02843e

rsc.li/nanoscale

Introduction

2D materials have shown great potential for device applications due to their intriguing properties and intrinsic quantum confinement effect. Among the experimentally explored 2D materials, SnSe sheets are of special interest. In 2014, bulk SnSe was found to possess the highest thermoelectric material efficiency.[1] Since then, increasing attention has been paid to SnSe sheets experimentally and theoretically to study the effect of dimensionality on the properties.[2–7] Subsequently, a single-layer SnSe sheet synthesized to form 2D materials[2,4] is found to be an indirect band gap semiconductor with many fascinating properties, such as a large negative Poisson's ratio, an ultralow lattice thermal conductivity (<3 W m^{-1} K^{-1} at 300 K), and a high carrier mobility of 11 000 cm^2 V^{-1} S^{-1} for holes,[7] which is comparable to that of graphene. In addition, compared with toxic lead, cadmium, or mercury containing minerals,[8,9] SnSe is an environmentally-friendly material with less pollution. All these features make single-layer SnSe sheets a promising candidate for electronic device applications.

For semiconductor devices, the interface properties of a semiconductor and its substrate are even more important than those of themselves. Ohmic contact is always desired due to the spontaneous charge carrier injection from the metal to the semiconductor. However, previous experimental work on the *I–V* curve of the Ag/bulk SnSe junction suggests a Schottky type contact with a barrier height of ~0.5 eV.[10] In addition to the bulk phase, Zhao *et al.* fabricated a field-effect transistor (FET) based on single-layer SnSe sheets showing an obvious current change at a bias voltage of 0.1 eV, which exhibits a smaller Schottky barrier of the contact than that of the bulk structure.[3] However, further theoretical study demonstrates that 2D SnSe sheets undergo a metallization when forming heterojunctions with 3D metals.[7] Such metallization leads to the Fermi level pinning,[11,12] resulting in ineffective modulation because the Schottky barrier height is almost completely insensitive to the work function of the metal electrode.

To weaken the strength of the Fermi level pinning, a new strategy is to use a 2D metal as the electrode in a contact to make the interaction at the junction interface be vdW force.[11,13] Such a technique has been applied to the MoS_2/graphene heterostructure, in which there is no metal induced gap states and the intrinsic properties of semiconductors are well preserved.[14–16] In this work, following the same idea of using 2D metals as the electrodes,[11] we study SnSe sheet-based vdW heterojunctions. We choose graphene as the electrode, which

[a]*Center for Applied Physics and Technology, Department of Materials Science and Engineering, HEDPS, Beijing Key Laboratory for Magnetoeletric Materials and Devices, College of Engineering, Peking University, Beijing 100871, China. E-mail: qianwang2@pku.edu.cn*
[b]*Collaborative Innovation Center of IFSA (CICIFSA), Shanghai Jiao Tong University, Shanghai 200240, China*

†Electronic supplementary information (ESI) available. See DOI: 10.1039/c8nr02843e

has been widely used to form vdW heterojunctions with other 2D semiconductors, such as phosphorene sheet,[15] 2D halide perovskites,[17] and penta-graphene.[18] Based on the geometrical structure of the SnSe/graphene (SnSe/G) heterojunction generated by using our in-house code to deal with the issue of lattice match between the single-layer SnSe sheet and graphene due to their different symmetries, we systematically study its electronic structure and band alignment, and evaluate its contact behavior. Besides H-NbS_2 and N-doped graphene as discussed in ref. 11, we further explore the tuning of the Schottky barrier using some other experimentally synthesized metallic 2D transition metal dichalchogenide (TMD) sheets including ZT-$MoSe_2$,[19–21] ZT-MoS_2,[22,23] and B-doped graphene. We then further study the modulation of the contact properties to realize Ohmic contact from Schottky contact.

Computational methods

Interface modelling

Because the lattice symmetry of the single-layer SnSe sheet and graphene is different, special care is needed in the construction of the heterostructure model in which the lattice mismatch strain should be minimized. To this end, we use our in-house code, which implements a supercell approach based on Zur and McGill's work[24] to generate the supercell models with a constraint of the lattice mismatch between the SnSe sheet and the graphene electrode of less than 2%. Simultaneously, we set the total number of atoms in the heterojunction to be less than 300, as it is difficult to deal with a large system in DFT calculations.

DFT calculations

Our calculations are based on density functional theory (DFT) as implemented in the Vienna *Ab initio* Simulation Package (VASP)[25,26] employing the projector augmented wave (PAW) pseudopotentials[26,27] and the Perdew–Burke–Ernzerhof (PBE) exchange–correlation functional.[28] To correctly describe the effect of van der Waals interaction, we use the dispersion-corrected DFT method (optB88-vdW).[29,30] The plane-wave cutoff energy is set to 400 eV for all the calculations. Monkhorst–Pack sampling[31] of sufficient *k*-points is used (see Table S1 in the ESI† for details). All studied heterostructures are fully relaxed until the energy and force on each atom are less than 0.0001 eV and 0.01 eV $Å^{-1}$, respectively. To obtain more accurate band gaps for the studied systems, we use the HSE06 functional[32,33] for the electronic structure calculations. Work functions are calculated by subtracting the corresponding electronic levels with respect to the vacuum level in the heterostructures.

Results and discussion

Geometry

By using our lattice match code, we obtain four SnSe/G heterostructures composed of a single-layer SnSe sheet and graphene with a constraint of the lattice match of less than 2%. The lattice parameters are given in Table S2 in the ESI,† which shows that the way to match two 2D surfaces is not unique. Our previous study demonstrates that the calculated results are insensitive to the supercell size.[18] Therefore, we choose the smallest model of the heterostructure in our calculations to reduce the computational cost.

The fully optimized geometry of the SnSe/G heterostructure is plotted in Fig. 1(a). We find that both the SnSe sheet and graphene remain almost intact without any obvious geometric distortions after optimization, implying that the lattice strain is indeed negligible in this heterostructure model. To examine its stability, we calculate the binding energy, which is defined as $E_b = -(E_H - E_G - E_{SnSe})/N$, where E_H is the total energy of the SnSe/G heterostructure, E_{SnSe} and E_G are the total energy of the freestanding SnSe and graphene sheets, respectively, and N is the number of carbon atoms in the graphene sheet. Fig. 1(b) shows the variation of binding energy per carbon atom as a function of the interlayer distance between the SnSe sheet and graphene. The equilibrium interlayer distance and the binding energy are found to be 3.48 Å and 57 meV, respectively, which are comparable to those of some vdW heterojunctions or crystals, such as 2D phosphorene/graphene (d = 3.45 Å, E_b = 60 meV),[15] graphite (d = 3.33 Å, E_b = 52 meV),[34] and hexagonal boron nitride (d = 3.33 Å, E_b = 65 meV).[34]

Contact evaluation

We first examine the electronic properties of the SnSe/G heterostructure. The projected band structures of SnSe/G on the SnSe sheet and graphene are calculated and plotted in Fig. 2(a) and (b), respectively. For the convenience of comparison, we also plot the band structures of the freestanding SnSe sheet and graphene, respectively, as shown in Fig. S1,† which are in good agreement with those of previous calculations.[5,7,35,36] We find that the energy band dispersions of both the freestanding SnSe sheet and graphene are almost completely preserved after being stacked together, which is an important feature of a vdW heterojunction. However, a close examination of the projected band structures uncovers that the valence band edge of SnSe is mixed with some states of graphene, which shifts the Fermi level of graphene up to 0.18 eV from the Dirac point, as shown in Fig. 2(b). We argue that the shift of the Fermi level is due to the formation of the interface dipole induced by the unsymmetrical charge distribution between the metal and the semiconductor surfaces. As shown in Fig. S2,† the charge distribution is asymmetrical between the two layers, leading to the formation of the interface dipole.

We then make a contact evaluation for this heterostructure. Fig. 3 shows the schematic diagram of a two-probe model for the SnSe/G heterojunction-based transistor. In this model, graphene acts as the metal electrode, while the SnSe sheet acts as the channel material. Typically, charge carriers encounter two energy barriers when they transport from the source to the channel region. One exists at the vertical interface of the contact, called the Schottky barrier ($\Phi_{SB\perp}$), which is the energy barrier for charge carrier transport across the interface of the

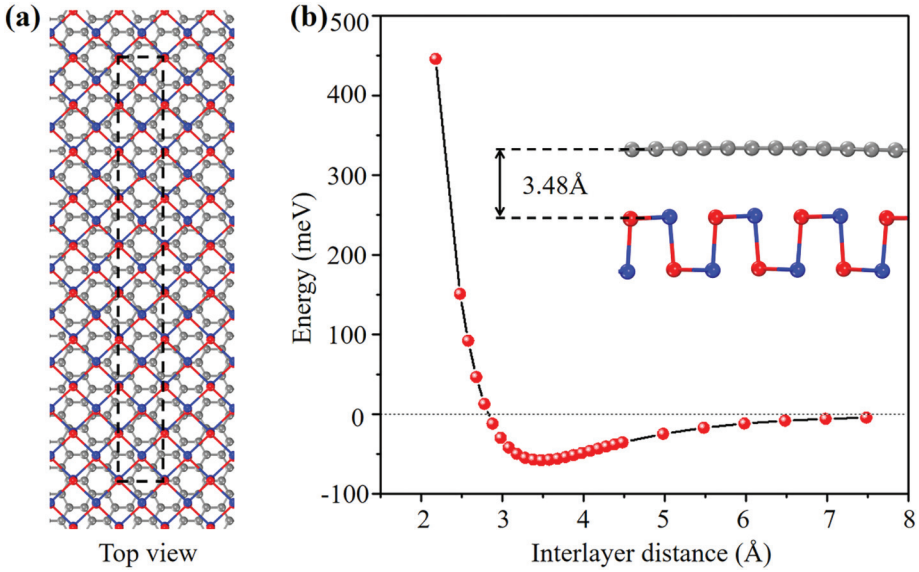

Fig. 1 (a) Top view of the optimized SnSe/G heterostructure. The black dashed-line rectangle represents the supercell of SnSe/G. (b) Variation of energy as a function of the interlayer distance between the SnSe sheet and graphene. The inset shows the side view of SnSe/G. Red, blue, and gray spheres represent Se, Sn, and C atoms, respectively.

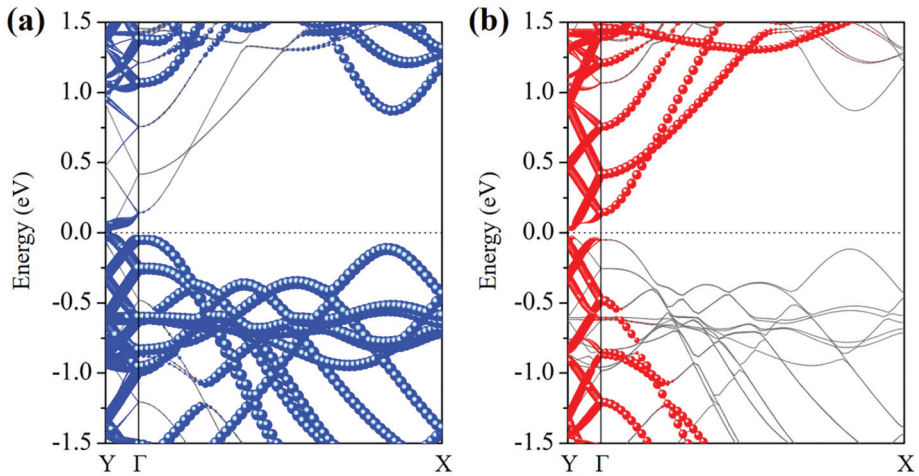

Fig. 2 Band structure of SnSe/G projected on (a) the SnSe sheet and (b) the graphene sheet.

SnSe/G heterojunction, and the other appears at the lateral interface between the contact and the channel part, characterized by band bending, ΔE_F. Both of these parameters are important in determining the performance of a FET device.

To calculate the band bending ΔE_F, we use the current-in-plane (CIP) geometry,[15,37] which is composed of the SnSe/G heterostructure and the freestanding SnSe sheet as the channel material in this study. The geometry and band alignment are plotted in Fig. 4. In a CIP geometry, a band bending usually occurs at the lateral interface due to the work function deference between the heterostructure and its channel material.[38] In this CIP geometry, the band bending is estimated by the Fermi level difference (ΔE_F) between that of the SnSe/G heterostructure and the freestanding SnSe sheet, *i.e.*, $\Delta E_F = W_H - W_{SnSe}$, where W_H and W_{SnSe} are their corresponding work functions, which are calculated to be 4.55 and 4.26 eV respectively, leading to a band bending (ΔE_F) of 0.29 eV, as shown in Fig. 4. Therefore, holes are the major carriers making the channel p-type as $\Delta E_F > 0$, similar to the case of the phosphorene/graphene-based device.[15]

To calculate the Schottky barrier ($\Phi_{SB\perp}$), we use the Schottky–Mott rule,[11] which defines $\Phi_{SB\perp}$ as the energy difference between the Fermi level of the heterojunction and its band edges:

$$\Phi_e = E_{CBM} - E_F, \Phi_h = E_F - E_{VBM} \quad (1)$$

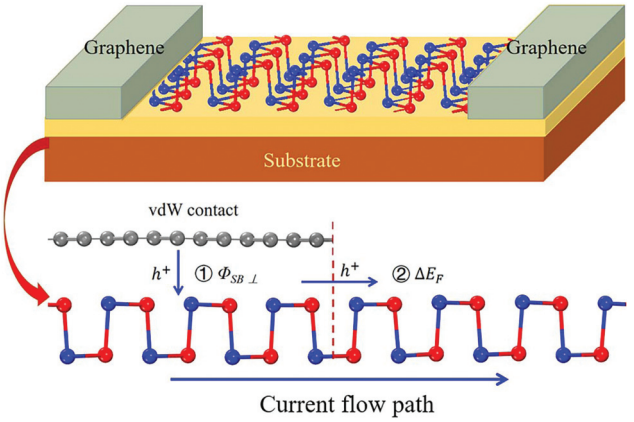

Fig. 3 Schematic diagram of a SnSe/G heterojunction-based transistor. $\Phi_{SB\perp}$ and ΔE_F represent the vertical Schottky barrier and the lateral band bending, respectively.

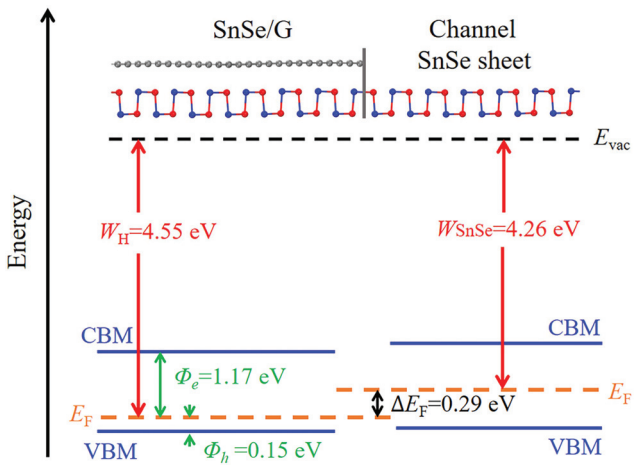

Fig. 4 Schematic diagram of the CIP geometry, and its corresponding band alignment. W_H and W_{SnSe} are the work functions of the SnSe/G heterostructure and the non-contacted SnSe sheet, respectively. E_{vac} represents the vacuum level.

where Φ_e and Φ_h are the Schottky barrier heights for electrons and holes, respectively, and E_F is the Fermi level of SnSe/G, while E_{CBM} and E_{VBM} denote the energies of the conduction band minimum (CBM) and the valence band maximum (VBM) of the SnSe sheet in the heterostructure, respectively. From the band alignment in Fig. 4, we obtain a $\Phi_{SB\perp}$ of 0.15 eV for holes. While the Au/SnSe sheet contact has a Schottky barrier height of 0.10 eV,[3] which is comparable to that of SnSe/G, the Au electrode has a much larger work function than that of the graphene one. Hence, the Fermi level pinning is weakened when the bulk Au is replaced by the graphene sheet.

Modulation of the Schottky barrier

For device applications, a small Schottky barrier or an Ohmic contact is ideal as the contact resistance can be reduced. According to the Schottky–Mott rule,[11] for a vdW heterostructure, the Schottky barriers of electrons and holes can be approximately calculated using

$$\Phi_{e\perp} = W - E_{EA}, \Phi_{h\perp} = E_{IP} - W \quad (2)$$

where W is the work function of the metal electrode, and E_{EA} and E_{IP} are the electron affinity and ionization potential of the semiconductor, respectively. The energy value of the difference between E_{IP} and E_{EA} is equal to that of the band gap of the semiconductor in the heterostructure. Eqn (2) can be derived from eqn (1) when the interaction between the semiconductor and the metal is negligible. Therefore, $\Phi_{SB\perp}$ can be modulated by tuning the work function of the metal electrode or changing the metal electrode with other materials having different work functions. Here, we use the two different approaches to modulate $\Phi_{SB\perp}$.

First, we tune $\Phi_{SB\perp}$ by doping the graphene sheet with boron (B) or nitrogen (N) atoms to change its work function. Because B and N are, respectively, located at the left and right of carbon in the periodic table, if one C atom is replaced by one B or N in a supercell of the SnSe/G heterostructure, the system will have one electron less or more. Thus, the work function of graphene can be changed, accordingly. We calculate the Fermi level of the B-doped graphene sheet, and find that it decreases to −4.11 eV from −3.59 eV, leading to an increase of the work function of 1.44 eV (from 4.42 eV to 5.86 eV). We then calculate the Schottky barrier $\Phi_{SB\perp}$ of the interface, and find that B doping shifts the Fermi level of the graphene sheet down to below the VBM of SnSe in the SnSe/G heterostructure, turning $\Phi_{SB\perp}$ from the Schottky type into the Ohmic one (see Fig. S3† for details). As mentioned above, 2D SnSe undergoes metallization when forming a heterojunction with 3D metal surfaces, resulting in $\Phi_{SB\perp}$ being insensitive to the metal work function.[10] However, the metal-induced gap states in the SnSe sheet are totally missing in this vdW heterostructure, thus leading to a tunable $\Phi_{SB\perp}$.

We then dope the graphene sheet with N atoms. We find that N doping raises the Fermi level resulting in a smaller work function as N has one electron more than C. Fig. 5(a) shows the variation of calculated work functions and $\Phi_{SB\perp}$ as a function of different doping concentrations for the SnSe/N-doped graphene heterostructure. We find that $\Phi_{h\perp}$ increases to 0.53 eV from the original value of 0.05 eV, while $\Phi_{e\perp}$ decreases to 0.46 eV from 0.87 eV when N doping concentration is increased from 1/64 to 2/64 in the supercell of the graphene sheet. If the doping concentration is further increased, the Fermi level of the heterostructure becomes closer to the CBM of the semiconductor SnSe, and consequently, the Schottky barrier changes from p-type to n-type, which means that the electron becomes the major charge carrier transporting from the N-doped graphene sheet to the SnSe sheet. According to previous study, the linear dependence of $\Phi_{SB\perp}$ on the metal work function should have a slope of ±1.[11] By linearly fitting these points, we obtain a slope of ±1.03, as shown in Fig. 5(a), implying that the Fermi level pinning is almost eliminated by N doping. The calculated electronic band structures and band alignments of the SnSe/

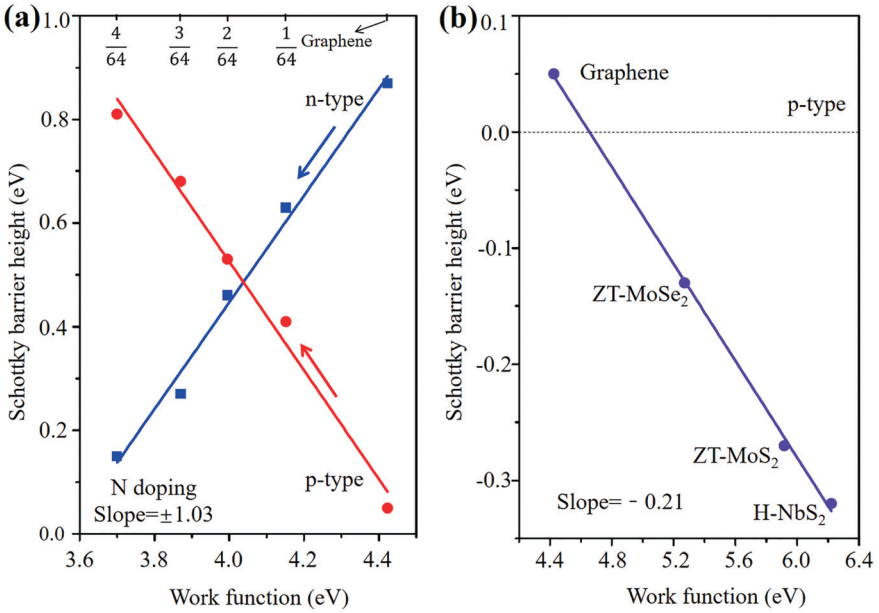

Fig. 5 Variation of the Schottky barrier height $\Phi_{SB\perp}$ and the work function with the N doping concentration for (a) SnSe/N-doped graphene and (b) SnSe/2D metal heterostructures. The top ticks in (a) represent the N-doping concentration.

N-doped graphene heterojunctions in each of the N concentrations studied are given in Fig. S4† for details.

Next, we tune the $\Phi_{SB\perp}$ by replacing the metal electrode (graphene) with some experimentally synthesized transition metal dichalchogenide (TMD) sheets, including ZT-$MoSe_2$, ZT-MoS_2, and H-NbS_2, respectively, because these 2D metals have larger work functions than that of graphene. The optimized geometric configurations and their corresponding lattice parameters of the considered supercells composed of the SnSe sheets and the TMD sheets are given in Fig. S5 and Table S3,† respectively. We calculate their band structures and band alignments (see Fig. S6† for details) and then calculate the Schottky barrier heights $\Phi_{SB\perp}$. As shown in Fig. 5b, the work functions are 5.27, 5.92, and 6.22 eV for the heterostructures with ZT-$MoSe_2$, ZT-MoS_2, and H-NbS_2 as the electrode, respectively, all of which are significantly greater than that of the heterostructure with graphene as the metal electrode (4.42 eV). Accordingly, the Fermi levels are shifted down to below the VBM by 0.13, 0.27, and 0.32 eV, respectively, leading to Schottky-barrier-free contacts with spontaneous hole injection from the metal to the semiconductor. For a clear view, we plot $\Phi_{SB\perp}$ for all the studied systems in Fig. S7† for comparison. One can see that a tunable Schottky barrier in the 2D SnSe-based heterojunctions can be achieved because the interaction between the metal electrode and the channel material is caused by the vdW force.

Conclusions

In summary, we systematically study the structural and electronic properties of a vdW heterostructure composed of a single layer SnSe sheet and graphene. We use our in-house code to construct a heterojunction supercell *via* minimizing the lattice mismatch, and use state-of-the-art theoretical calculations to evaluate the contact performance including the lateral band bending and vertical Schottky barriers. Our main results include: (1) the electronic properties of both the SnSe sheet and graphene are almost completely conserved after being stacked together, indicating that the interaction between the two surfaces is caused by vdW forces; (2) a positive band bending appears at the lateral interface; (3) different from the strong Fermi level pinning in 2D SnSe sheet/3D metal contacts, the metal-induced gap states are totally suppressed due to the vdW interaction, leading to a tunable Schottky barrier height Φ_{SB}; (4) an Ohmic contact can be realized by doping graphene with B atoms or replacing graphene with other high-work-function 2D metals, leading to spontaneous hole injection from the metal to the semiconductor. These findings solve the problem of the un-tunable Schottky barrier height of 2D SnSe/3D metal contacts, which plays a significant role in future device fabrications.

Conflicts of interest

There are no conflicts to declare.

Acknowledgements

This work is partially supported by grants from the National Natural Science Foundation of China (NSFC-51471004 and NSFC-21773004), and the National Key Research and Development Program of China (2016YFE0127300 and

2017YFA0205003), and supported by the High Performance Computing Platform of Peking University, China.

References

1 L.-D. Zhao, S.-H. Lo, Y. Zhang, H. Sun, G. Tan, C. Uher, C. Wolverton, V. P. Dravid and M. G. Kanatzidis, *Nature*, 2014, **508**, 373.
2 L. Li, Z. Chen, Y. Hu, X. Wang, T. Zhang, W. Chen and Q. Wang, *J. Am. Chem. Soc.*, 2013, **135**, 1213–1216.
3 S. Zhao, H. Wang, Y. Zhou, L. Liao, Y. Jiang, X. Yang, G. Chen, M. Lin, Y. Wang and H. Peng, *Nano Res.*, 2015, **8**, 288–295.
4 C. Tan and H. Zhang, *Nat. Commun.*, 2015, **6**, 7873.
5 F. Q. Wang, S. Zhang, J. Yu and Q. Wang, *Nanoscale*, 2015, **7**, 15962–15970.
6 K. Tyagi, K. Waters, G. Wang, B. Gahtori, D. Haranath and R. Pandey, *Mater. Res. Express*, 2016, **3**, 035013.
7 L.-C. Zhang, G. Qin, W.-Z. Fang, H.-J. Cui, Q.-R. Zheng, Q.-B. Yan and G. Su, *Sci. Rep.*, 2016, **6**, 19830.
8 A. Scheuhammer, *Environ. Pollut.*, 1987, **46**, 263–295.
9 A. Mews, A. Eychmüller, M. Giersig, D. Schooss and H. Weller, *J. Phys. Chem.*, 1994, **98**, 934–941.
10 H. Şafak, M. Şahin and Ö. F. Yüksel, *Solid-State Electron.*, 2002, **46**, 49–52.
11 Y. Liu, P. Stradins and S.-H. Wei, *Sci. Adv.*, 2016, **2**, e1600069.
12 Y. Pan, Y. Wang, M. Ye, R. Quhe, H. Zhong, Z. Song, X. Peng, D. Yu, J. Yang and J. Shi, *Chem. Mater.*, 2016, **28**, 2100–2109.
13 A. K. Geim and I. V. Grigorieva, *Nature*, 2013, **499**, 419–425.
14 L. Yu, Y.-H. Lee, X. Ling, E. J. Santos, Y. C. Shin, Y. Lin, M. Dubey, E. Kaxiras, J. Kong and H. Wang, *Nano Lett.*, 2014, **14**, 3055–3063.
15 J. Padilha, A. Fazzio and A. J. da Silva, *Phys. Rev. Lett.*, 2015, **114**, 066803.
16 Y. Liu, H. Xiao and W. A. Goddard, *J. Am. Chem. Soc.*, 2016, **138**, 15853–15856.
17 Y. Guo, W. A. Saidi and Q. Wang, *2D Mater.*, 2017, **4**, 035009.
18 Y. Guo, F. Q. Wang and Q. Wang, *Appl. Phys. Lett.*, 2017, **111**, 073503.
19 N. D. Boscher, C. J. Carmalt, R. G. Palgrave, J. J. Gil-Tomas and I. P. Parkin, *Chem. Vap. Deposition*, 2006, **12**, 692–698.
20 D. Kong, H. Wang, J. J. Cha, M. Pasta, K. J. Koski, J. Yao and Y. Cui, *Nano Lett.*, 2013, **13**, 1341–1347.
21 H. Li, L. Chen, Y. Zhang, X. Ji, S. Chen, H. Song, C. Li and H. Tang, *Cryst. Res. Technol.*, 2014, **49**, 204–211.
22 M. Chhowalla, H. S. Shin, G. Eda, L.-J. Li, K. P. Loh and H. Zhang, *Nat. Chem.*, 2013, **5**, 263–275.
23 K.-K. Liu, W. Zhang, Y.-H. Lee, Y.-C. Lin, M.-T. Chang, C.-Y. Su, C.-S. Chang, H. Li, Y. Shi and H. Zhang, *Nano Lett.*, 2012, **12**, 1538–1544.
24 A. Zur and T. McGill, *J. Appl. Phys.*, 1984, **55**, 378–386.
25 G. Kresse and J. Furthmüller, *Phys. Rev. B: Condens. Matter*, 1996, **54**, 11169–11186.
26 G. Kresse and D. Joubert, *Phys. Rev. B: Condens. Matter*, 1999, **59**, 1758.
27 P. E. Blöchl, *Phys. Rev. B: Condens. Matter*, 1994, **50**, 17953.
28 J. P. Perdew, K. Burke and M. Ernzerhof, *Phys. Rev. Lett.*, 1996, **77**, 3865.
29 J. Klimeš, D. R. Bowler and A. Michaelides, *J. Phys.: Condens. Matter*, 2009, **22**, 022201.
30 J. Klimeš, D. R. Bowler and A. Michaelides, *Phys. Rev. B: Condens. Matter*, 2011, **83**, 195131.
31 H. J. Monkhorst and J. D. Pack, *Phys. Rev. B: Solid State*, 1976, **13**, 5188.
32 J. Heyd, G. E. Scuseria and M. Ernzerhof, *J. Chem. Phys.*, 2003, **118**, 8207–8215.
33 J. Heyd, G. E. Scuseria and M. Ernzerhof, *J. Chem. Phys.*, 2006, **124**, 219906.
34 G. Graziano, J. Klimeš, F. Fernandez-Alonso and A. Michaelides, *J. Phys.: Condens. Matter*, 2012, **24**, 424216.
35 M. Gmitra, S. Konschuh, C. Ertler, C. Ambrosch-Draxl and J. Fabian, *Phys. Rev. B: Condens. Matter*, 2009, **80**, 235431.
36 G. Gui, J. Li and J. Zhong, *Phys. Rev. B: Condens. Matter*, 2008, **78**, 075435.
37 K. Gong, L. Zhang, W. Ji and H. Guo, *Phys. Rev. B: Condens. Matter*, 2014, **90**, 125441.
38 D. Xian-Qi, W. Xiao-Long, L. Wei and W. Tian-Xing, *Chin. Phys. B*, 2015, **24**, 117308.

